

# Seismic Resilience Assessment for Steel-Concrete Composite Bridges Including Impacts of Near-Fault Earthquakes

Yang Liu<sup>1</sup>; Da-Gang Lu<sup>2</sup>; Fabrizio Paolacci<sup>3</sup>; Gianluca Quinci<sup>3,\*</sup>; and Sourabh Vern<sup>3</sup>

Submitted: 18 January 2024 Accepted: 03 June 2024 Publication date: 03 September 2024

DOI: 10.70465/ber.v1i1.5

**Abstract:** This paper proposes a seismic resilience assessment method for steel-concrete composite bridges (SCCB) considering near-fault earthquake hazards. Based on conventional probabilistic seismic hazard disaggregation analysis, a correction factor is defined to represent the proportion of the occurrence probability of the near-fault pulse-like, near-fault non-pulse-like and far-field earthquake conditioned on a given intensity level concerning the total occurrence probability of all earthquakes. The parameters of functionality recovery functions are modified using the factor proposed, and then the restoration processes after each type of earthquake are estimated. Correspondingly, vulnerabilities of a typical SCCB under near-fault and far-field earthquakes are developed as a case study. Based on the seismic hazard and fragility results, the seismic risk for each type of earthquake in a 50-year horizon is estimated. After that, the modified functionality recovery function is derived from the expected functionality. To implement the proposed method, the expected seismic resilience indices of a typical SCCB involved in the SEQBRI project are estimated, and the seismic resilience assessment is conducted. The seismic resilience assessment without considering earthquake type is also conducted for comparison analysis using the same bridge. The result shows that the seismic resilience of bridges in near-fault earthquake scenarios can be analyzed by the method proposed, and reducing the structural vulnerability under low-intensity level earthquakes and improving the structural recovery efficiency for slight and moderate damage states are more meaningful to enhance the seismic resilience of bridges.

**Author keywords:** Seismic resilience; occurrence probability; steel-concrete composite bridges; near-fault earthquakes assessment

## Introduction

The concept of seismic resilience has been recently employed to explore the post-earthquake behavior of civil and industrial infrastructure conditions in terms of recovery cost and time.<sup>1,2</sup> In general, seismic resilience is defined as the ability of a system to mitigate hazards, contain the effects of natural disasters, and carry out recovery activities in such a way as to minimize social disruption and reduce the impact of future earthquakes.<sup>3</sup> While seismic risk is strictly related to the capacity and robustness of a construction against earthquake, seismic resilience is instead associated with post-earthquake recovery conditions that typically include direct

and indirect economic losses.<sup>3,4</sup> In this respect, the uncertainties related to the seismic vulnerability and the recovery phase suggest the use of a probabilistic approach for the resilience estimation.<sup>1,3,5,6</sup>

The fundamental framework of probabilistic resilience assessment proposed by several authors is illustrated in Fig. 1.<sup>3,7</sup> In particular, the conventional seismic risk analysis under the framework of Performance-based Earthquake Engineering (PBEE) is the basis of the risk assessment methodology. It includes a) probabilistic seismic hazard analysis, b) seismic fragility analysis, and c) loss and robustness estimation. The formulation of a Probabilistic Seismic Resilience Analysis (PSRA) methodology required the introduction of concepts like recovery estimation and resilience assessment.<sup>2,8,9</sup>

This approach has been largely applied in the literature for the quantitative resilience assessment of bridges under seismic loading. Most of these works were mainly focused on the effects of the seismic vulnerability of structural components<sup>10,11</sup> or the recovery functions<sup>12,13</sup> on the bridge resilience. Moreover, several novel methodologies were proposed to quantify the seismic resilience of a bridge by using reliability concepts and fuzzy mathematics.<sup>14,15</sup> Furthermore, the assessment of time-dependent resilience of a

\*Corresponding Author. Gianluca Quinci.

Email: gianluca.quinci@uniroma3.it

<sup>1</sup>College of Civil Engineering & Architecture, Wenzhou University, Wenzhou 325035, P.R. China

<sup>2</sup>School of Civil Engineering, Harbin Institute of Technology, Harbin 150090, P.R. China

<sup>3</sup>Department of Civil, Computer Science and Aeronautical Technologies Engineering, Roma Tre University, Rome 00146, Italy

Discussion period open till six months from the publication date. Please submit separate discussion for each individual paper. This paper is a part of the Vol. 1 of the International Journal of Bridge Engineering, Management and Research (© BER), ISSN 3065-0569.

bridge<sup>16,17</sup> and the resilience assessment of transportation have also been developed by Reed et al.<sup>18</sup> and Ouyang et al.,<sup>19</sup> which was also supported by monitoring of the resilience framework by Quinci et al.<sup>20</sup>.

Nonetheless, the seismic resilience of bridges located in the near-fault region has not been sufficiently investigated, even though near-fault earthquakes can generate severe damages,<sup>21,22</sup> (Alavi et al. (2001), Billah et al. (2013)). Consequently, in the present paper, a refined approach for assessing the seismic resilience of bridges in near-fault regions is proposed, which is strongly based on a PSRA approach. The following issues have been analyzed: 1) Probabilistic seismic hazard disaggregation analysis considers the difference between near-fault and far-field earthquake hazards. Besides, the respective hazard of near-fault pulse-like and non-pulse-like earthquakes is computed using a proportionality coefficient derived from the PSHA analysis through the velocity pulse method,<sup>23</sup> (Baker (2007)), 2) the pulse-like and non-pulse-like ground motions records are identified for the fragility analysis, 3) the empirical functionality recovery functions are modified to include the impact of near-fault earthquakes. 4) Based on these steps, a revised formula of expected seismic functionality is provided for the probabilistic seismic resilience assessment.

Thus, the purpose of this study is twofold: 1) to introduce a refined assessment method of seismic resilience of bridges in near-fault regions, and 2) to evaluate the importance of considering near-fault earthquakes in resilience assessment. To this end, firstly, a brief review of the current approach for the resilience assessment of bridges that do not include near-fault effects is offered in Section 2, whereas the proposed method is described in Section 3. Then, as an illustrative example, the seismic resilience of a new type of steel-concrete bridge is investigated in Section 4 using the proposed method. Furthermore, the same example is used to compare near-fault and far-field conditions in the resilience assessment.

## Probabilistic seismic resilience assessment methods

### Classical approach

The general definition of resilience is the following<sup>3,5,7,18,24</sup>:

$$R = \frac{\int_{t_0}^{t_0+T_T} Q(t)dt}{T_T} \quad (1)$$

where  $R$  is the resilience;  $Q(t)$  is the functionality recovery function depending on time  $t$ ;  $t_0$  is the occurrence time of the earthquake;  $T_T$  is the full functionality recovery time interval, which is derived as the summation of the idle time interval  $T_I$  and the recovery time interval  $T_R$ .  $T_I$  and  $T_R$  are two recovery parameters that directly affect resilience. The residual functionality  $Q_r$  at time  $t_0$  and the target functionality  $Q_t$  are other important recovery parameters. An illustration of resilience and recovery parameters is offered in Fig. 2.

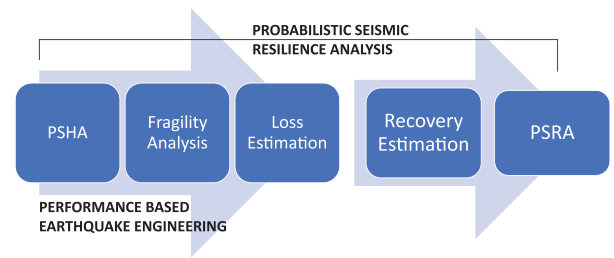


Figure 1. The fundamental framework of seismic resilience assessment

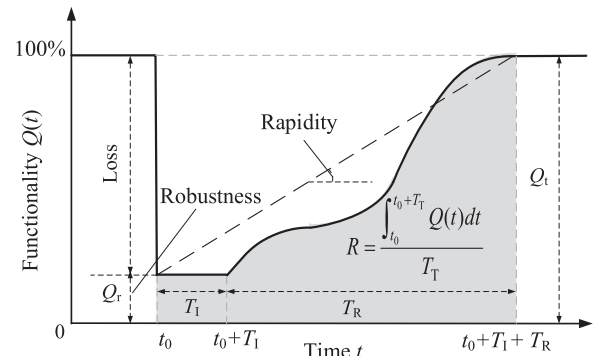


Figure 2. Fundamental concepts of seismic resilience

Rapidity and robustness are the two key properties of resilience.<sup>5</sup> Rapidity is defined as the slope of the functionality curve during the recovery time  $t$ . Given its time-varying nature, an average recovery rate is preferred, which is denoted as  $RA$ , as shown in Fig. 2, whose definition is the following<sup>7</sup>:

$$RA = \frac{Q_t - Q_r}{T_T} \quad (2)$$

Robustness, here denoted as  $RO$ , is the ratio between the residual functionality at the time  $t_0$  and the full functionality (shown in Fig. 2).

The fundamental framework for predicting the seismic resilience of a bridge, as shown in Fig. 1, comprises five main stages.<sup>25</sup> The loss estimation is beyond the scope of this paper and will not be treated. The other four stages, probabilistic seismic hazard analysis (PSHA), seismic fragility analysis (SFA), recovery estimation, and probabilistic seismic resilience analysis (PSRA), are herein briefly introduced. The outcome of the PSHA is the probability of occurrence of a seismic event with intensity  $IM=i$  at the site where the bridge is located.<sup>26</sup> It is herein denoted as  $P_H$  ( $IM = i$ ).

In the fragility analysis of the bridge, the damage is classified into different states (i.e., slight, moderate, extensive, and complete), and the vulnerability is represented by the probability of the bridge being in the specific damage states (DSs) at each level of  $IM$  is quantified. Using the index  $j$  to distinguish the different DSs, the vulnerability can be expressed as  $P_V(DS = j | IM = i)$ .

The recovery function estimation can be carried out according to the statistics on specific bridge rehabilitation procedures after earthquakes. The functionality associated with the serviceability condition is usually expressed as a

normalized value (e.g., 100% of the traffic capacity with no earthquake occurrence or the goal for a completed recovery). The mostly used functionality recover function has been proposed in Cimellaro et al.,<sup>7</sup> and it is expressed by Eq. (3):

$$Q(t) = 1 - L(t) = Q_r + H(t) \cdot f_r(t) \quad (3)$$

where  $L(t)$  measures the loss of functionality at time  $t$ ;  $Q_r$  is the residual functionality at time  $t_0$ ;  $H(t)$  is the Heaviside step function;  $f_r(t)$  is the recovery function at time  $t$ . In recent contributions, several typical simplified recovery functions have been proposed, such as the trigonometric model in Chang and Shinozuka,<sup>27</sup> the exponential model in Kafali and Grigoriu,<sup>28</sup> the linear model in Bruneau and Reinhorn,<sup>6</sup> Cimellaro et al.<sup>5</sup> and Ouyang et al.<sup>19</sup>. Bocchini et al.<sup>24</sup> proposed a comprehensive recovery function containing the four recovery parameters presented in Fig. 2. This function will be adopted here by synthesizing these three recovery functions.

The recovery procedure is usually divided into several phases, which can be expressed by the Heaviside step function,  $H(t)$ .<sup>7</sup> The main parameters of the  $H(t)$ , the idle and the recovery time interval, can be obtained through the statistical analysis approach based on functionality evaluation data.<sup>1</sup> The residual functionality  $Q_r$  can be assessed by a complete damage investigation and the corresponding loss analysis. For the end condition of the recovery procedure, the target functionality  $Q_t$  can be decided by administrators or be equal to 100% for a convenient assumption.

In this study, the functionality recovery function for different  $DS$ s is denoted as  $Q_j(t)$ , where  $j$  refers to the  $j$ -th damage state. Note that, for each  $Q_j(t)$ , there is a corresponding idle time interval  $T_I$ , recovery time interval  $T_R$ , residual functionality  $Q_r$ , and target functionality  $Q_t$ .

To quantify the seismic resilience in the last PSRA stage of the method, the expected functionality  $\bar{Q}(t)$  can be obtained by using the following expression<sup>11</sup>:

$$\bar{Q}(t) = \sum_{i=1}^{n_{IM}} P_H(IM = i) \sum_{j=1}^{n_{DS}} P_V(DS = j | IM = i) Q_j(t) \quad (4)$$

where  $P_H(IM = i)$ ,  $P_V(DS = j | IM = i)$  and  $Q_j(t)$  are the hazard, fragility curve and functionality recovery function, respectively. By substituting Eq. (4) in Eq. (1), the seismic resilience of the bridge can be quantified.

### Proposal of a method for the resilience assessment of bridges in near-fault conditions

For bridges in near-fault regions, which may suffer more serious seismic damages,<sup>22</sup> an improved approach to assess the probabilistic seismic resilience is herein presented. This approach allows us to distinguish the effects of near-fault and far-field earthquakes based on their probability of occurrence. Moreover, two types of the near-fault ground motions (pulse-like and non-pulse-like ground motions) are further distinguished. Accordingly, the fundamental framework of Fig. 1 can be re-thought as illustrated in Fig. 3.

(1) Probabilistic Seismic Hazard Analysis (PSHA). The aim of this part is to acquire the occurrence probability

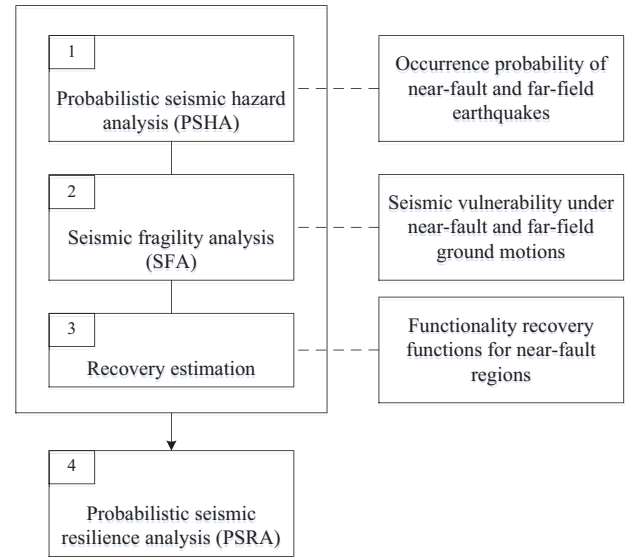


Figure 3. Flowchart of the PSRA in near-fault regions

of the near-fault pulse-like (NFPL), near-fault non-pulse-like (NFNP), and far-field (FF) earthquakes for each level of IM. A convenient method to obtain the probability of occurrence of specific seismic events using the existing data of probabilistic seismic hazard disaggregation (PSHD) is proposed. Firstly, the  $P_H(IM=i)$  can be calculated using the classic seismic hazard curves. Then, the occurrence probability of the three types of earthquakes for each level of IM can be evaluated by using the following equation in which the parameter  $s$  is a proportion factor.

$$P_S(ST = k | IM = i) = s(ST = k | IM = i) \cdot P_H(IM = i) \quad (5)$$

where  $ST$  is the abbreviation for seismic event type;  $k$  can assume the values 1,2 or 3 if the seismic event is of type NFPL, NFNP, and FF, respectively;  $s(ST=k|IM=i)$  is a factor obtained by PSHD, which indicates the proportion of the occurrence probability of the specific type of earthquake conditioned on the intensity  $i$  with respect to the total occurrence probability of all earthquakes  $P_H(IM=i)$ .

The conventional PSHD provides the contribution of all possible sources to the probability of exceeding each intensity measure IM,<sup>29,30</sup> as shown in Fig. 4, where the classical deaggregation plot is illustrated.<sup>30</sup> The total contribution of near-fault sources to the seismic hazard can be calculated by summing the contributions satisfying the condition that the closest distance of the site from the fault ( $Rcd$ ) is lower than or equal to 20 km.<sup>22,31</sup>

Similarly, the contribution of far-field sources can be obtained. With this approach, the ratio of specific seismic hazard (NF or FF) to the total one is obtained. By transforming the probability of exceedance to the occurrence probability, the percentage of NF and FF seismic events for the selected intensity  $IM=i$  can be calculated, which are herein indicated as  $s_N(IM=i)$  and  $s_F(IM=i)$ , respectively. For example,  $s_F$  means  $s(ST=3|IM=i)$ .

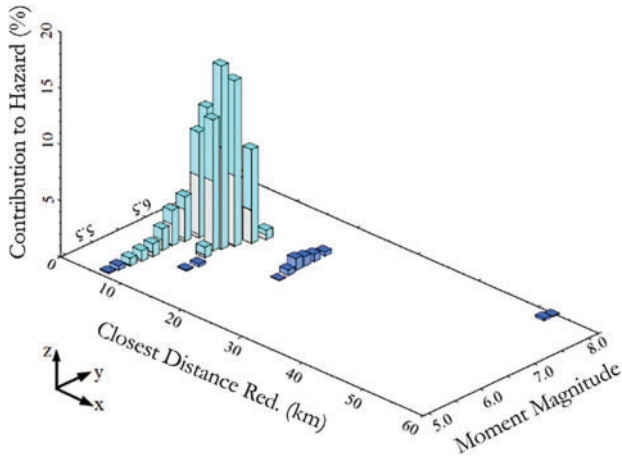


**Figure 4.** Example of the probabilistic seismic hazard disaggregation<sup>32</sup>

The proportion factor  $s(ST=k|IM=i)$  for NFPL and NFNP is calculated as,

$$s(ST = k | IM = i) = \alpha_k(IM = i) \cdot s_N(IM = i) \quad k = 1, 2 \quad (6)$$

where  $\alpha_k(IM=i)$  indicates the percentage of the total probability that a near-fault source generates pulse-like ( $k=1$ ) or non-pulse-like ( $k=2$ ) seismic events conditioned to  $IM=i$ . Referring to the PSHD approach presented in Shahi et al.,<sup>31</sup> the values of the  $\alpha_k(IM=i)$  could be determined by statistics to historical seismic records at a specific source.

(2) **Seismic Fragility Analysis (SFA).** In this step, the vulnerability function, here denoted as  $P_V(DS = j | IM = i)$ , need to be refined accounting for the specific type of ground motion ( $ST=1,2,3$ ) earthquakes, that is  $P_{V,ST=k}(DS = j | IM = i)$ . To separate the pulse-like and non-pulse-like ground motions, the quantitative identification method for velocity pulse is here adopted.<sup>23,33</sup> This latter is based on the idea of adopting a simplified numerical model of the real ground motion calibrated through the least-square fitting (LSF) technique. Subsequently, an energy index (Ep) is defined and calculated to identify the pulse-like ones among the selected natural earthquake records. According to Zhai et al.,<sup>33</sup> the ground motions can be considered pulse-like when the value of Ep is greater than 0.3.

(3) **Recovery estimation.** In this stage, the functionality recovery function for each damage state  $Q_j(t)$  is differentiated by near-fault and far-field earthquakes. Even though the probability distribution of the parameters in  $Q_j(t)$  is generally unknown, the data of the real procedure of bridge functionality restoration can be gathered and used to provide empirical values of the recovery parameters, including minimum, moderate, and maximum values.<sup>1</sup> Given that, for a given IM, the seismic damage states of the bridge under near-fault ground motions usually differ from those caused by far-field ground motions,<sup>22</sup> the recovery curves corresponding to different damage states are different. So, it is reasonable to assume that the recovery function parameters' values correlate to the hazard of NF and FF earthquakes.

To be more specific, the smaller residual functionality ( $Q_r$ ), the longer idle time ( $T_I$ ), and the recovery time ( $T_R$ ) should be used to account for the impact of NF ground motions. Hence, by using the percentage of the NF and FF earthquakes, the modified moderate values of the parameter in  $Q_j(t)$  for each damage state and for each IM are assumed as follows:

$$V_{r,m}(DS = j | IM = i) = \frac{s_N(IM = i) \cdot V_{r,max}(DS = j) + s_F(IM = i) \cdot V_{r,min}(DS = j)}{s_N(IM = i) + s_F(IM = i)} \quad (7)$$

where  $V_{r,m}(DS = j | IM = i)$  represents the modified moderate values of recovery parameters for  $DS=j$  conditioned on  $IM=i$ ,  $V_{r,max}(DS=j)$  and  $V_{r,min}(DS=j)$  represent the maximum and minimum values of the recovery parameters. The weight of the maximal and minimal values to the modified values are the percentage of NF and FF earthquakes,  $s_N(IM=i)$  and  $s_F(IM = i)$ .

It is worth noting that the most severe damage to bridges may be induced by the NF earthquake event rather than the FF earthquake; hence, the most adverse values of recovery parameters (for example, the longest recovery time and the minimal residual functionality) in the functionality recovery function should result from the NF condition.<sup>22,33</sup> Consequently, for the parameter  $Q_r$ ,  $V_{r,max}(DS=j)$  should be assumed as the minimal absolute value, whereas  $V_{r,min}(DS=j)$  is the maximum absolute one. On the contrary, for the parameters  $T_I$  and  $T_R$ ,  $V_{r,max}(DS=j)$  should assume the maximum absolute value and the  $V_{r,min}$  as the absolute minimum one.

(4) **Probabilistic Seismic Resilience Analysis (PSRA).** After the three previous stages, the expected functionality level  $\bar{Q}(t)$  in Eq. (5) can be rewritten as:

$$\bar{Q}_{RE}(t) = \sum_{i=1}^{n_{IM}} \sum_{k=1}^{n_{ST}} P_S(ST = k | IM = i) \sum_{j=1}^{n_{DS}} P_{V,ST=k}(DS = j | IM = i) Q_{DS=j|IM=i}(t) \quad (8)$$

where  $P_S(ST = k | IM = i)$ ,  $P_{V,ST=k}(DS = j | IM = i)$ , and  $Q_{DS=j|ST=k}(t)$  are those obtained from the previous stages. Then, the assessment of the bridge resilience in a near-fault region is completed by substituting  $\bar{Q}_{RE}(t)$  into Eq. (1). In addition, the robustness and rapidity of the refined expected resilience can be calculated following the method presented in section 2.1.

## Illustrative example

### Description of the numerical model

Short-medium span steel-concrete composite bridges made of hot-rolled beams and concrete cross beams are very common in non-seismic areas due to the economic benefits of limiting manufacturing and short construction time. To extend this favorable structural solution to high seismic-prone areas, and therefore, cover the relevant lack of

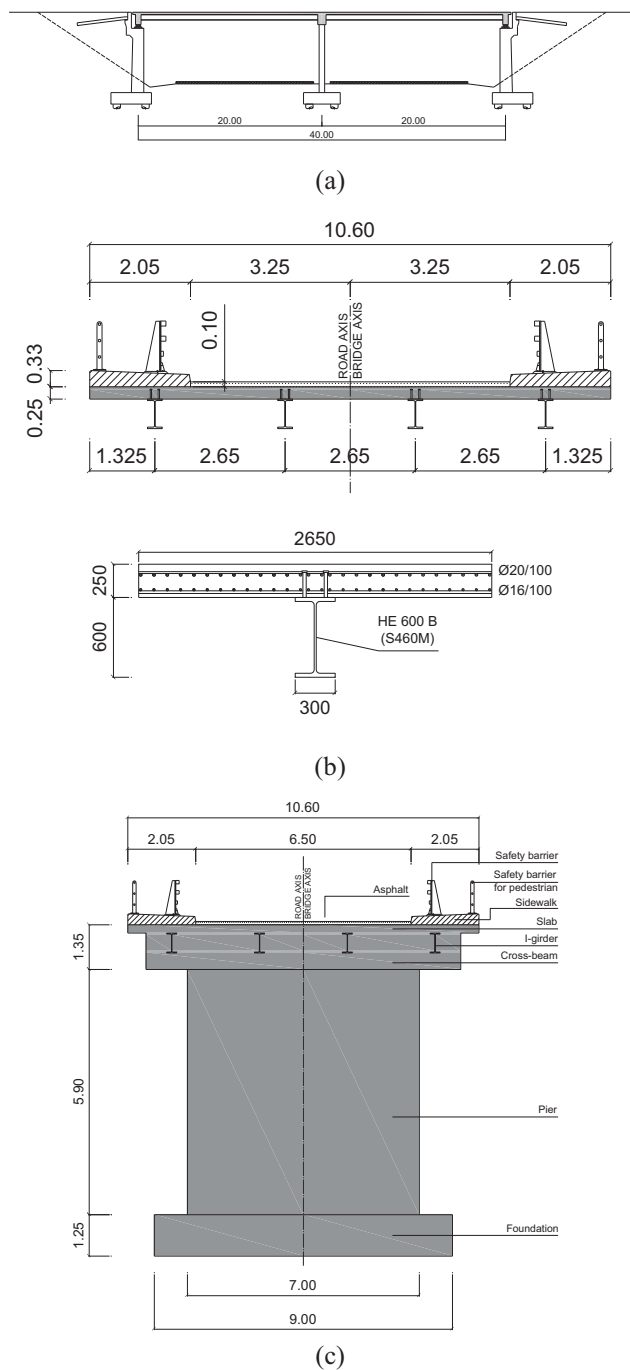


**Figure 5.** Illustrative example: (a) frontal view bridge; (b) Deck composite concrete-steel girder, (c) Wall Pier

knowledge on the seismic response of these types of bridges, a wide research activity has been carried out within the European Project SEQBRI.<sup>34</sup> In this respect, a two-span concrete-steel composite road overpass can be applied, or the proposed resilience assessment methodology can be applied.

The analyzed bridge is a typical highway overpass designed according to Eurocodes.<sup>35</sup> It is characterized by two spans of 20.00 m, a total width of the road cross-section equal to 10.60 m, with a carriageway 6.50 m wide and two sidewalks 2.05 m wide, as shown in Fig. 5. The concrete slab is 0.25 m thick, and it is supported by four main I-girders

HLB 600 sections made with hot-rolled S460 steel, with 2.65 m in-between distance. The deck-to-pier connection is of monolithic type because of the presence of Concrete Cross Beams (CCB) with sections 60 × 90, as shown in Fig. 5. The CCBs are designed according to Chabrolin et al.<sup>36</sup> At the abutments, the steel girders are connected to the CCB, which is 0.60 m wide, and the deck is simply supported on normal damping rubber bearings. At the intermediate pier, a monolithic pier-to-deck connection is adopted in which the pier is fixed to a reinforced CCB 0.90 m wide (Fig. 4). The connection between steel girders and abutments and between steel girders and intermediate pier is guaranteed by 0.60 m and 0.90 m wide reinforced CCB, respectively. The pier height is 7.00 m, with a 0.60x7.00 m transversal section, and a deep foundation for the piers is chosen. To minimize the construction phases of the steel-concrete composite deck, a procedure based on one-step pouring has been adopted. The foundation soil is assumed to be categorized as type B according to CEN<sup>37</sup> and the soil structure interaction effect is neglected.

The 3D finite element (FE) model has been developed using the collaborative framework OpenSees.<sup>38</sup> This model uses force-based nonlinear beam elements with fiber cross-sections to model the single steel girder and the tributary concrete slab. The Menegotto–Pinto model<sup>39</sup> is adopted to simulate the mechanical behavior of steel girders and slab reinforcement, while the Kent–Park<sup>40</sup> model is used to reproduce the mechanical behavior of concrete. Nonlinear links with elastoplastic behavior are used to model the shear studs connecting the steel girders to the slab, within the CCB, and along the deck.

Fig. 6 shows the details of the 2-D FE model for the concrete crossbeam. Rigid links are used to model the vertical head plate, which is welded on the steel girders and directly in contact with the transverse concrete beam. Different nonlinear links modeling the behavior of the horizontal shear-headed studs within the joint are connected to these rigid links according to the CCB configuration.

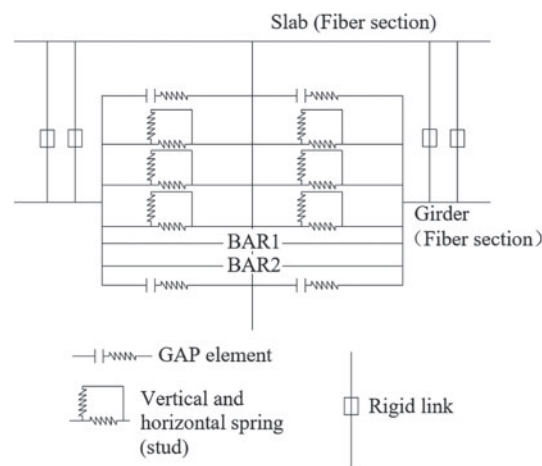


**Figure 6.** 2-D FE model of the beam-to-pier connections

To simulate the constraint in compression due to the presence of the CCB, gap elements are adopted at both the left and right sides of the CCB joint at two different heights,

as shown in Fig. 6. A simplified procedure for evaluating the stiffness of the gap elements is performed, if the compression force transferred by the girder will exert uniformly on the contact area of the vertical head plate. Two groups of the prestressing bars at the bottom area of the CCB are modeled by two elastic truss elements. More details can be found in Liu et al.<sup>41</sup>.

The strength of the shear studs has been evaluated in accordance with CEN,<sup>42</sup> while the stiffness has been evaluated using the load-slip curves experimentally defined by Gattesco and Giuriani.<sup>43</sup> The behavior of the CCB joint is difficult to reproduce. A component-based model proposed by Paolacci et al.<sup>34</sup> has been adopted to represent the behavior of the CCB. Details of the novel type of pier-to-deck connections can be found in Abbiati et al.,<sup>44</sup> which is beyond the scope of this study.

### Probability of occurrence of earthquakes in near-fault regions

According to the performance-based earthquake engineering approach, the use of Intensity Measures (IMs) that enable consistent hazard conditions and exhibit a strong correlation with the selected quantity of interest has been extensively debated in the literature. The most accepted procedure is based on selecting a global IM that can be used to scale the selected records to exceed difference limit states. The suitability of a selected IM depends on the nature of the dynamic problem.<sup>45,46</sup> Frequently used IMs are generally scalar and often identified with the peak ground acceleration (PGA) or the spectral acceleration at a given vibration period ( $S(T)$ ) of the structure. This latter has often been demonstrated to be superior with respect to PGA,<sup>47,48</sup> and hence will be employed in this paper for the seismic resilience assessment. In the following, it will be simply indicated as  $S_a$ .

For the probabilistic seismic hazard disaggregation analysis, the Interactive disaggregation tool<sup>30</sup> has been adopted to achieve the factors ( $ST = k$ ) at the given location of bridges and the site condition. The bridge is assumed to be ideally located in the city of Livermore in California (USA), with a northern latitude of 37.682° a western longitude of 121.768°, which is a recognized near-fault seismic region according to the Interactive Fault Map available in the U.S. Geological Hazard Science Center.<sup>49</sup> The seismic design conditions belong to the NEHRP site class B/C boundary, with an average shear-wave velocity in the top 30 meters m/s. ( $V_s^{30}$ ) of 760 m/s.<sup>50</sup>

The contributions of seismic hazard associated with the exceedance probability of 1%, 2%, 5%, 10%, 20%, and 50% in 50 years have been calculated, and the corresponding  $S_a$  are respectively equal to 0.94g, 0.78g, 0.58g, 0.45g, 0.33g, and 0.19g. Subsequently, the ratios  $S_N(IM=i)$  and  $S_F(IM=i)$  can be obtained by using the site-to-source distance of 20 km to categorize the source type into far-field (FF) and near-fault (NF).

As described in Section 2, a near-fault pulse-like (NFPL) source is characterized by the presence of velocity pulses in the velocity time history of ground motions. The recommended values of  $\alpha_k(IM=i)$  in Eq. (6), i.e., the proportion

factor for NFPL, are respectively 65%, 70%, 75%, 80%, 85%, and 90%, which corresponds to the level of IM from small to large.<sup>51,52</sup> Fig. 7 shows the proportion of FF, NFNP, and NFPL sources with respect to the total source contributions.

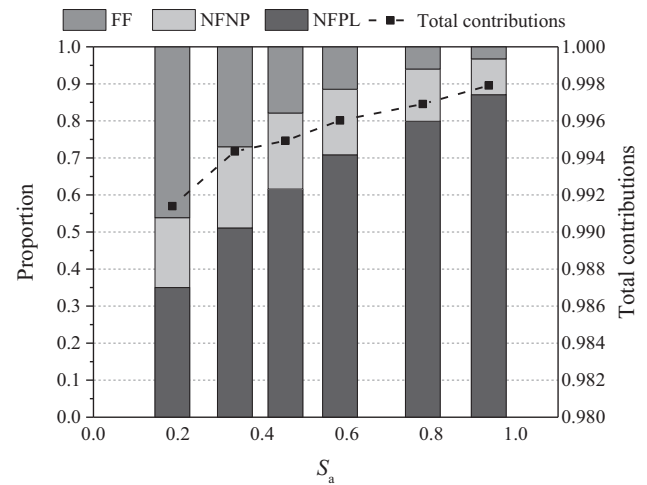


Figure 7. Proportion of FF, NFPL, and NFNP ground motions<sup>53</sup>

It can be noted that the proportion of NF sources increases from 55% to 97% as the IM level increases. This is why separately considering the occurrence probability of near-fault earthquakes can reduce the errors for resilience assessment. Because the mean hazard for several ground-motion prediction equations is adopted in the PSHD, the total contribution at each level of IM is not 100%, as shown in Fig. 7. The value of the total contribution is always greater than 99%, which basically satisfies the analysis needs in this study.

The hazard curves of the site, for a reference life of 50 years, have been provided by the United States Geological Survey (2017). The probability of occurrence of seismic events with a given intensity IM,  $P_H(IM=i)$ , are determined and used in Eq. (5) along with the value of  $s(ST=k|IM=i)$  shown in Fig. 7. Finally, the probability of occurrence  $P_S(ST = k | IM = i)$  of NFPL, NFNP, and FF earthquakes is computed.

### Selection of ground motions

For the fragility analysis of the bridge, a suite of ground motions representative of NF and FF ground motions have been selected using the PEER strong ground motion database of NGA-West2.<sup>54</sup> When selecting NF ground motions, the following hazard conditions are considered: moment magnitudes ( $M_W$ ) greater than 6.0 and site-to-source distances ( $R$ ) less than 20 km., and the NF earthquakes with the ratio of peak ground velocity (PGV) and peak ground acceleration (PGA) being greater than 0.2.<sup>55,56,33,57</sup> The FF ground motion records were selected to match the PGA and  $M_W$  of the NF records but with  $R > 20$  km. To satisfy the assumption of NEHRP site class B/C and the assumption of  $V_s^{30}$  value in the 537-1150 m/s range for more optional ground motion records.

Due to the limited number of NFNP ground motion records, only eight ground motion records were selected. Hence, the number of the ground motion records for NFPL and FF is eight, considering the record-to-record variability.<sup>26,58</sup> All selected ground motions were recorded during the following eight strong earthquake events: San Fernando earthquake (USA, 1971), Nahanni earthquake (Canada, 1985), Loma Prieta Earthquake (America, 1989), Manjil Earthquake (Iran, 1990), Northridge Earthquake (America, 1994), Chi-Chi Earthquake (Taiwan, 1999), Kocaeli Earthquake (Turkey, 1999), Lwate Earthquake (Japan, 2008).

It has been recognized that the velocity pulse included in the velocity time history of the ground motion is the most important feature of the NFPL ground motion.<sup>31</sup> For a certain pulse-like ground motion, its biggest velocity pulse is generated along the strike parallel direction and the strike normal direction. Therefore, the strike parallel and normal components of the selected pulse-like ground motion are used for fragility analysis. Using the wavelet method,<sup>23,51,59</sup> identified the pulse-like ground motions and calculated the

two components of these pulse-like ground motions, which are provided in the PEER database.

The ground motions selected for this study are listed in Table 1, where  $R$  represents the site-to-source distance,  $M_w$  represents the moment magnitude,  $PGA$  represents the peak ground acceleration, and  $S_a(T_1, 5\%)$  represents the spectral acceleration at the first period with a 5% damping ratio.

### Seismic fragility analysis

If the seismic demand ( $D$ ) and capacity ( $C$ ) follow a log-normal distribution, the fragility represented by the failure probability can be expressed in the following form Cornell et al.<sup>26</sup>:

$$P(D \geq C | IM) = \Phi \left[ \frac{\ln(m_{D|IM}) - \ln(m_C)}{\sqrt{\beta_{D|IM}^2 + \beta_C^2}} \right] \quad (9)$$

where  $m_{D|IM}$  and  $\beta_{D|IM}$  are, respectively, the median and dispersion of the demand obtained numerically through time-history analysis;  $m_C$  and  $\beta_C$  are the median and the dispersion of the capacity obtainable through numerical

**Table 1.** The selection of ground motion records

Ground motion	Event No.	NGA No.	Station, component	$R$ (km)	$M_w$	$PGA$ (g)	$S_a(T_1, 5\%)$ (g)
NFPL	1	763	Gilroy - Gavilan Coll, strike parallel	9.96	6.93	0.35	0.21
	2		Gilroy - Gavilan Coll, strike normal			0.33	0.32
	3	1161	Gebze, strike parallel	10.92	7.51	0.26	0.17
	4		Gebze, strike normal			0.14	0.24
	5	1511	TCU076, strike parallel	2.74	7.62	0.34	0.72
	6		TCU076, strike normal			0.43	0.37
	7	1529	TCU102, strike parallel	1.49	7.62	0.30	0.45
	8		TCU102, strike normal			0.17	0.84
NFNP	9	495	Site 1, 010	9.6	6.76	1.10	0.46
	10		Site 1, 280			1.19	0.73
	11	496	Site 2, 240	4.93	6.76	0.51	0.29
	12		Site 2, 330			0.36	0.50
	13	1517	TCU084, EW	11.48	7.62	1.01	2.30
	14		TCU084, NS			0.43	1.14
	15	1521	TCU089, EW	9	7.62	0.35	0.49
	16		TCU089, NS			0.23	0.37
FF	17	72	Lake Hughes #4	25.07	6.61	0.18	0.36
	18	989	LA - Chalon Rd	20.45	6.69	0.20	0.70
	19	1234	CHY086	28.42	7.62	0.17	0.40
	20	1485	TCU045	26	7.62	0.49	0.31
	21	87	Santa Anita Dam	30.7	6.61	0.19	0.14
	22	1633	Abbar	40.4	7.37	0.52	1.00
	23	5659	IWTH27	43.59	6.9	0.27	0.12
	24	5680	MYGH04	40.43	6.9	0.20	0.08

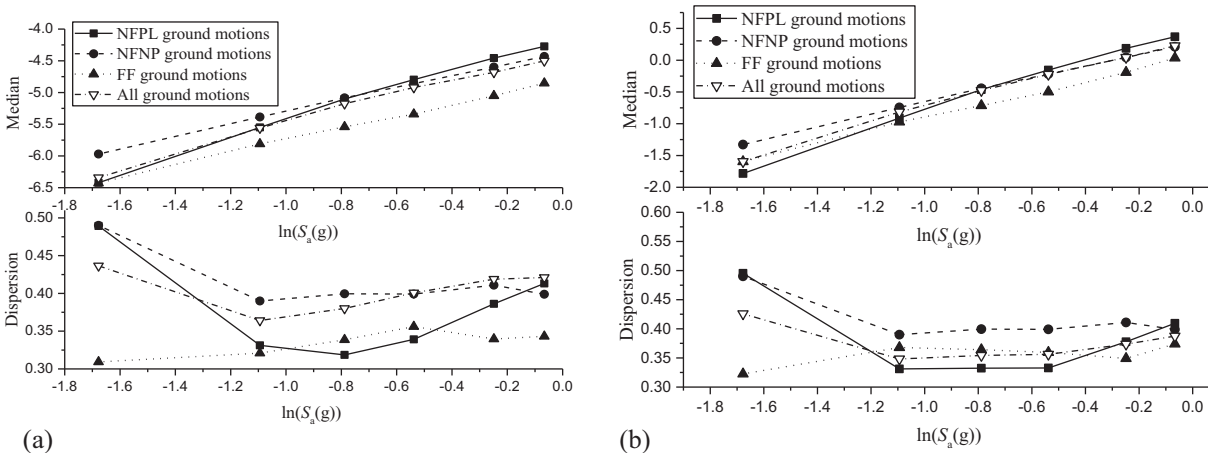


**Figure 8.** Medians and dispersions of demand: (a) pier drift ratio, (b) pier curvature ductility

analysis (i.e., push-over analysis) or experimental investigations;  $\Phi(\bullet)$  is the standard normal cumulative distribution function. This study considers the record-to-record variability associated with the seismic action in the probabilistic seismic demand analysis (PSDA). Moreover, the uncertainties associated with the structural response and the capacity are considered in the probabilistic seismic capacity analysis (PSCA).

Accordingly, the PSDA of the bridge is performed through Multiple Stripe Analysis (MSA) by Tothong et al.<sup>60</sup>. The levels of IM are selected based on PSHD results presented in Section 3.2. The ground motions are then modified by scaling the values of  $S_a$  to match the selected IM. Consequently, a total of 144 nonlinear time-history analyses have been performed. The pier drift ratio (ratio of the maximum displacement of the pier top and the total height of the pier,  $DR$ ) and the pier displacement ductility (ratio of the maximum displacement and the yielding displacement of the pier,  $\delta_p$ ) have been used as Engineering Demand Parameters (EDP). This choice derives from the preliminary analysis, which indicated that significant damage in the CCB appears only for high seismic intensity values, whereas the most significant one is located on the pier.<sup>61</sup> In addition, given that the selected bridge's transversal response is smaller than the longitudinal one, only this latter has been analyzed.<sup>61</sup>

A log-log representation of the probabilistic seismic demand model has been assumed here, as suggested by Conell et al.<sup>26</sup>. Accordingly, the natural logarithm of EDP depends linearly on the  $\ln(IM)$ . As stated before, to reduce the dispersion  $\beta_{DIM}$ ,<sup>62,63</sup> the demand parameters ( $m_{DIM}$  and  $\beta_{DIM}$ ) have been obtained separately for NFPL, NFNP, and FF ground motions and only for comparison, also for the entire set of ground motions.

Fig. 8 shows the median and dispersion of demand in terms of pier drift ratio and pier curvature ductility at each level of IM. It can be easily noted that they are higher for NFPL and NFNP ground motions with respect to FF signals. It can be noticed that both mean values of pier drift and curvature at the base section are higher when near fault condition is considered, and more in particular for NFPL

condition, when  $S_a > 0.45$  g ( $\ln S_a > 0.8$ ). For lower values of  $S_a$  the NFNP condition prevails. In any case, the differences are limited.

As stated before, the pier is the most vulnerable element of the bridge, with potentially catastrophic consequences. Usually, piers experience different degrees of damage, from the cover spalling and fracture to the buckling of longitudinal reinforcement and, finally, bars fracture. These four damage levels are selected as Damage Measures (DMs) and will be associated with slight, moderate, extensive, and complete damage conditions. Damage state thresholds (limit states) for typical bridges with wall-type piers have been defined in the literature using damage analysis combined with experimental tests and numerical simulations.<sup>64</sup> Table 2 summarizes the mean values and the dispersions of the different limit states. Using these values, the fragility curves for slight, moderate, extensive, and complete damage have been obtained by Eq. 9, illustrated in Fig. 11, for example, in terms of pier drift ratio and displacement ductility and for slight damage and moderate damage conditions.

The graph shown in Fig. 11 represents the probability of exceedance at each level of IM for NFPL, NFNP, FF, and all ground motions. These data points are linked by straight lines for the lack of reliable data at the other seismic intensities. Note that the results of the seismic fragility for both two EDPs are too obviously different to present the

**Table 2.** Damage states for pier of wall type and dispersions of capacity.

	Slight damage	Moderate damage	Extensive damage	Complete damage
Drift ratio ( $DR$ )	0.36%	0.72%	1.87%	3.30%
Displacement ductility ( $\mu_D$ )	1.029	2.177	4.187	8.373
Dispersion of capacity ( $\beta_C$ )	0.488	0.542	0.538	0.605

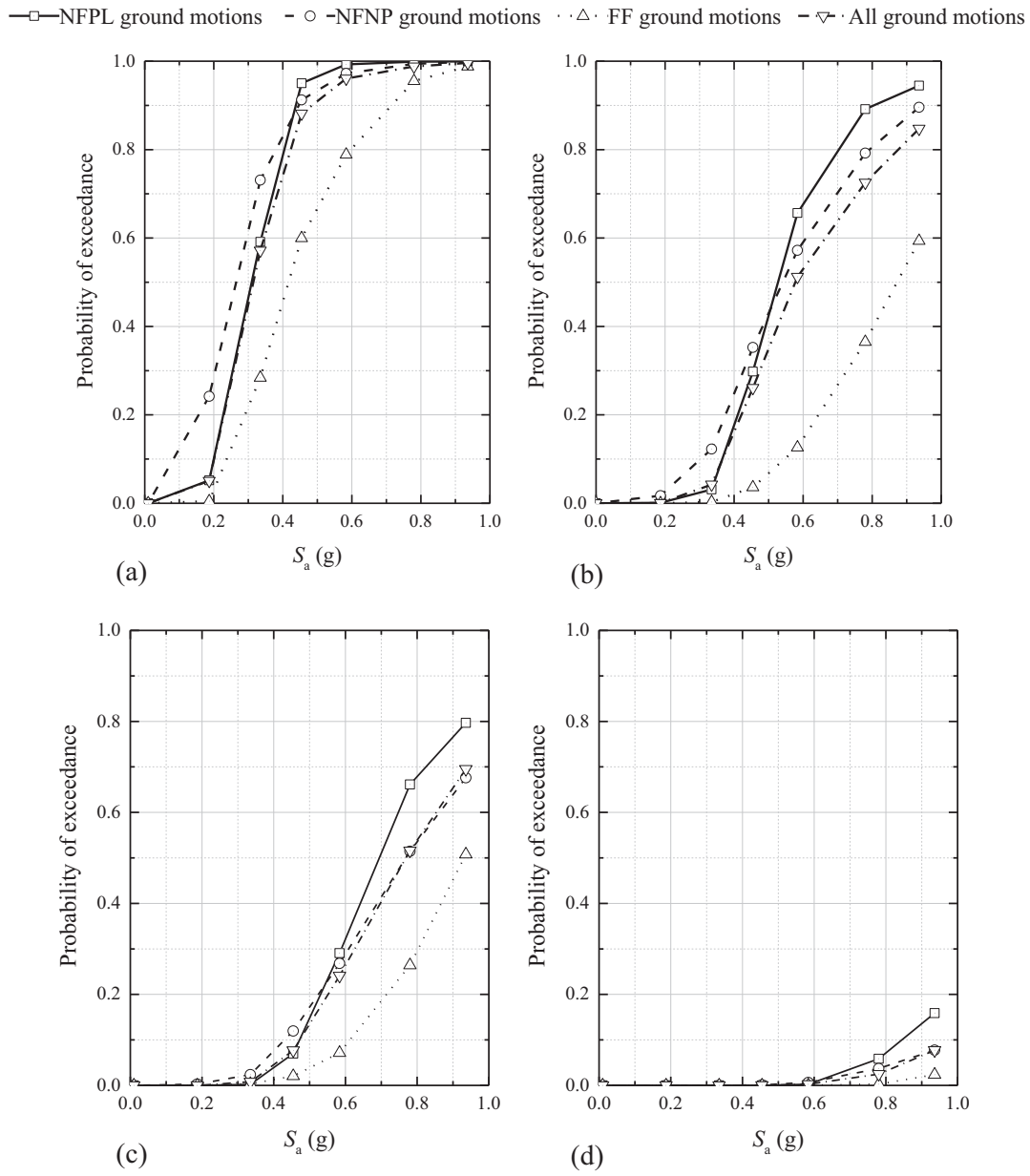


**Figure 11.** Component fragility curves for pier drift ratio of (a) slight damage, (b) moderate damage, and for displacement ductility of (c) slight damage, (d) moderate damage

fragility of the whole bridge; the system fragility curves combined with all components are adopted here. Based on the conservative assumption of the tandem connection between components,<sup>63</sup> the system fragility can be expressed as:

$$Fragility_{\text{system}} = 1 - \prod_{c=1}^{n_{\text{component}}} [1 - Fragility_c] \quad (10)$$

in which the  $n_{\text{component}}$  is the number of components considered in the analysis, and  $c$  is the specific component. By applying Eq. (10), the system fragility is obtained. To be more effective in the representation of the probability, Table 3 reports the probability to be exactly in a specific damage state DS, defined as the difference between the fragilities of two sequential damage states:

$$P(D = D_{\text{slight}}) = P(D \geq D_{\text{moderate}}) - P(D \geq D_{\text{slight}}) \quad (11)$$

For example, in Table 3 for the NFPL ground motions, when  $S_a=0.19g$ , there is only a 0.1% probability of moderate damage occurring, while there is a 5.1% probability of slight damage, and the level of damage does not continue to get larger. When  $S_a=0.94g$ , there is only a 4.6% probability that slight damage will occur and will not continue to develop. In contrast, there is a 71.2% probability that the slight damage will develop to the moderate damage state, a 22.3% probability that it will develop to a severe state, and a 1.8% probability that it will develop to a complete state. Thus, it can be understood that the total probability of damage, or the probability of all having slight damage, is about 99.9%.

In this way, it is easy to identify the conditions where a damaged state prevails. For example, the higher the  $S_a$ , the lower the probability of being exactly in a slightly damaged

**Table 3.** System vulnerability in different damage states.

Type of ground motions	$S_a$ (g)	Slight damage	Moderate damage	Extensive damage	Complete damage
NFPL	0.19	0.051	0.001	0.000	0.000
	0.45	0.656	0.298	0.000	0.000
	0.94	0.046	0.712	0.223	0.018
NFNP	0.19	0.227	0.017	0.000	0.000
	0.45	0.570	0.351	0.003	0.000
	0.94	0.096	0.775	0.124	0.005
FF	0.19	0.005	0.000	0.000	0.000
	0.45	0.572	0.036	0.000	0.000
	0.94	0.391	0.598	0.006	0.000
All	0.19	0.050	0.001	0.000	0.000
	0.45	0.630	0.260	0.001	0.000
	0.94	0.140	0.751	0.103	0.005

**Table 4.** Empirical values of recovery parameters according to the literature<sup>65,66,67</sup>

Damage state	Residual functionality (%)			Idle time (months)			Recovery time (months)			$A$	$s$
	Moderate	Max	Min	Moderate	Max	Min	Moderate	Max	Min		
Light	75	100	50	1.5	2	1	2.667	5	0.333	0.0	0.5
Moderate	25	50	0	1.5	2	1	3.667	6.667	0.667	-0.1	0.5
Extensive	10	20	0	1.5	2	1	5.167	8.333	2	0.1	0.5
Complete	0	0	0	1.5	2	1	6.25	10	2.5	0.1	0.5

state condition. This probability is the highest for  $S_a < 0.45g$ , but it decreases for higher  $S_a$ .

For the sake of brevity, only three seismic intensities are shown in Table 3.

### Functionality recovery model

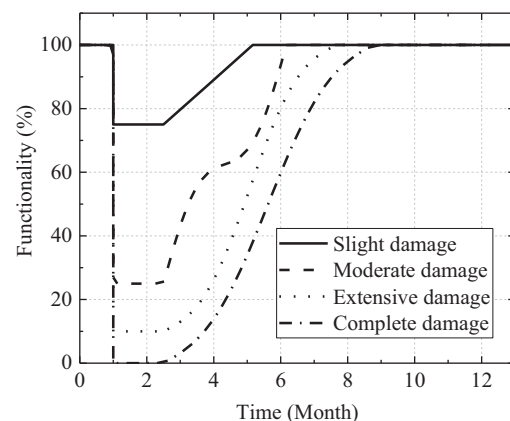
In this section, the parameters of the functionality recovery functions for the four damage states are estimated by the method presented in Section 2.2. Empirical values for the three recovery parameters of the residual functionality, idle time, and recovery time can be determined based on the evaluation of data from the real functionality recovery of bridges in California as listed in Table 4,<sup>65,66</sup> referred to as the same damage parameters of Table 2. The values of the shape parameters (defined as  $A$  and  $s$ ) recommended by Dong et al.<sup>17</sup> for the recovery functions based on engineering experience are also reported in Table 4. Parameter  $A$  governs the amplitude of the sinusoidal function, and parameter  $s$  defines the flex position of the sinusoid, as defined by Bocchini et al.<sup>24</sup>.

In addition, the target functionality is assumed to be constant and equal to 100% for each damage state. Fig. 9 shows the recovery empirical functions for the four damage states according to the values of Table 4. The curves of Fig. 9 have been obtained by applying Eq. (7). The parameters of the functionality recovery empirical functions are reported in Table 5.

### Resilience estimation and discussion

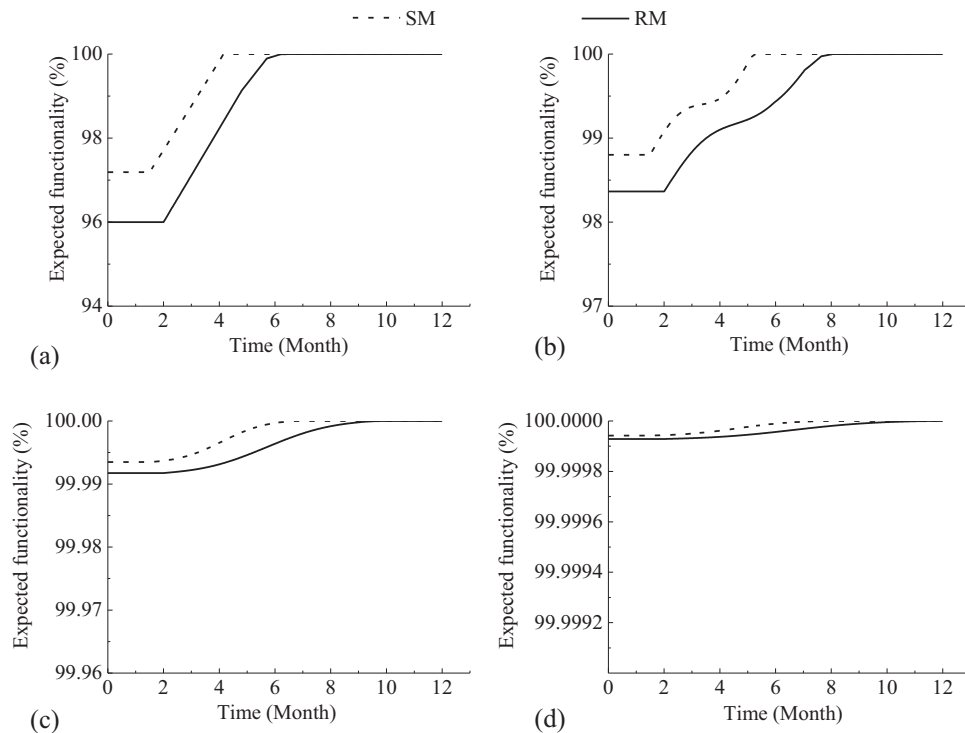
According to the refined method (RM) presented in Section 2.2, the expected functionality of the bridge in 50 years can be calculated by applying Eq. (8), which includes the effects of NF earthquakes. A simplified method (SM) also estimates the functionality without distinguishing NF from FF conditions.

Fig. 10 illustrates the expected functionality of the bridge for each damage state, estimated by considering both conditions (RM and SM). It can be noted that the corresponding

**Figure 9.** Empirical functionality recovery profiles

**Table 5.** Values of refined recovery parameters for functionality recovery empirical functions

	Damage state	$S_a$ (g)					
		0.19	0.33	0.45	0.58	0.78	0.94
Residual functionality (%)	Slight	73	63	59	56	53	52
	Moderate	23	13	9	6	3	2
	Extensive	9	5	4	2	1	1
	Complete	0	0	0	0	0	0
Idle time (months)	—	1.5	1.7	1.8	1.9	1.9	2.0
Recovery time (months)	Slight	2.8	3.7	4.2	4.5	4.7	4.8
	Moderate	3.9	5.0	5.6	6.0	6.3	6.5
	Extensive	5.4	6.6	7.2	7.6	8.0	8.1
	Complete	6.5	8.0	8.7	9.1	9.6	9.8



**Figure 10.** Expected functionality in 50 years of (a) slight damage, (b) moderate damage, (c) extensive damage, and (d) complete damage

recovery paths are different. For each damage state, the RM condition is related to a lower residual functionality and a longer recovery time. The difference is reduced in extensive and complete damage conditions, as shown in Fig. 10 (c) and (d). This results from the low probabilities associated with strong events and severe damage. For the quantitative assessment of the seismic resilience in near-fault conditions, the expected resilience index,  $R$ , is adopted here to assess seismic resilience in near-fault conditions quantitatively. Using Eq. (1), the  $R$  for each IM and damage state level is calculated using RM and SM conditions, respectively. Because, as already observed, the differences between NFPL and NFNP are limited, we omitted these two cases for brevity to distinguish in Fig. 10.

The results are listed in Table 6, in which the relative errors are also presented in brackets. Although strong earthquakes and serious damage could reduce the resilience of the bridge, in engineering practice, the low probability of a strong seismic event and the reduced vulnerabilities of extensive or complete damage states more strongly affect seismic resilience. Therefore, the expected resilience index of complete damage and that for the seismic event of 0.94g are close to 100%. Comparison analysis results of RM and SM show that the values of the estimated seismic resilience of RM are smaller than that of SM. The relative errors, computed as the difference between methods of non-distinguishing and distinguishing NF and FF events, are in the range of 0 to

**Table 6.** Expected resilience matrix of the bridge and relative errors for two methods.

$S_a$ (g)	Expected resilience (%)							
	Slight damage		Moderate damage		Extensive damage		Complete damage	
	RM	SM	RM	SM	RM	SM	RM	SM
0.19	98.98	99.78(0.81)	99.66	100.00(0.41)	100	100.00(0.00)	100	100.00(0.00)
0.33	96.92	99.34(2.50)	99.42	99.82(0.40)	100	100.00(0.00)	100	100.00(0.00)
0.45	98.85	99.89(1.06)	99.26	99.71(0.46)	99.89	99.99(0.10)	100	100.00(0.00)
0.58	99.89	99.89(0.10)	99.71	99.94(0.23)	99.97	100.00(0.03)	100	100.00(0.00)
0.78	100	100.00(0.00)	99.98	100.00(0.02)	100	100.00(0.00)	100	100.00(0.00)
0.94	100	100.00(0.00)	100	100.00(0.00)	100	100.00(0.00)	100	100.00(0.00)

**Table 7.** Expected Resilience of the bridge and the relative errors of rapidity and robustness

$S_a$ (g)	Resilience (%)		Relative error of rapidity (%)	Relative error of robustness (%)
	RM	SM		
0.19	98.70	99.62(0.94)	-16.82	0.33
0.33	95.42	98.89(3.63)	-5.31	0.85
0.45	97.49	99.40(1.97)	2.17	0.46
0.58	99.43	99.87(0.44)	7.77	0.10
0.78	99.97	99.99(0.03)	4.28	0.00
0.94	100.00	100.00(0.00)	-1.76	0.00
Aggregate result (Combined all intensities)	94.01	97.77(4.00)	8.95	2.12

3%. The maximum relative error of 2.5% appears when the bridge is slightly damaged at the level of IM 0.33g.

Though the difference between the two methods presented in Table 6 is limited, the aggregated seismic resilience of all investigated damage states and all levels of IM may lead to higher relative errors. The aggregated expected resilience at each level of IM for both MR and SR conditions is listed in the second and third columns of Table 7, along with the relative error in terms of rapidity and robustness. The maximal relative error in the expected resilience is found at  $IM = 0.33g$ , equal to 3.63%. In any case, the relative errors are limited when the intensity of seismic events is larger than 0.5g. By aggregating all the levels of IM, the resilience of the bridge calculated in MR condition becomes 94.01% with an error of 4.00% with respect to SM. In terms of robustness, RM provides lower values, which indicates that the results of RM are more conservative. The relative error in rapidity is large, especially for lower IM (16.82%), even though non-regular behavior can be noticed when IM varies.

To better understand the effects of NF and FF conditions on the expected resilience, the proportion of the NF earthquakes is changed in the range -50% - +50%. This way, it is intended to locate the bridge in different NF regions. The reason for selecting variations in percentage and not in absolute values of NF and FF proportions is to investigate in a clear manner the sensitivity of the bridge resilience with respect to initial conditions derived by predefined seismic hazard conditions.

The expected resilience, rapidity, and robustness results are illustrated in Fig. 12 for the case RM. Relative errors of the results calculated from the new proportions. It is found that the maximum relative error of the expected resilience is 1.8%, while that of the rapidity and robustness are almost 15% and 2%, respectively. In the investigated range of this study, the variation tendency of the resilience decreases along with the increasing occurrence proportion of NF earthquakes. Combining the results shown in Table 7 and Fig. 12, it can be concluded that the maximum relative error for the expected resilience of RM to SM is nearly 10%, at least for the selected case study.

It should be emphasized that the recovery parameters are random variables, though the refined moderate values are used in this study. With this respect, the maximum relative errors of the expected resilience, including the uncertainties of recovery parameters, can be magnified to more than 20% based on the engineering experience and analysis result. Consequently, a larger relative error can occur in SM condition in comparison with RM, reaching the value for the case study of about 15%.

## Conclusions

A refined approach for probabilistic seismic resilience assessment has been presented for bridges in near-fault regions. The impact of near-fault ground motions is considered using probabilistic seismic hazard disaggregation results. According to the selected case study, a steel-concrete composite

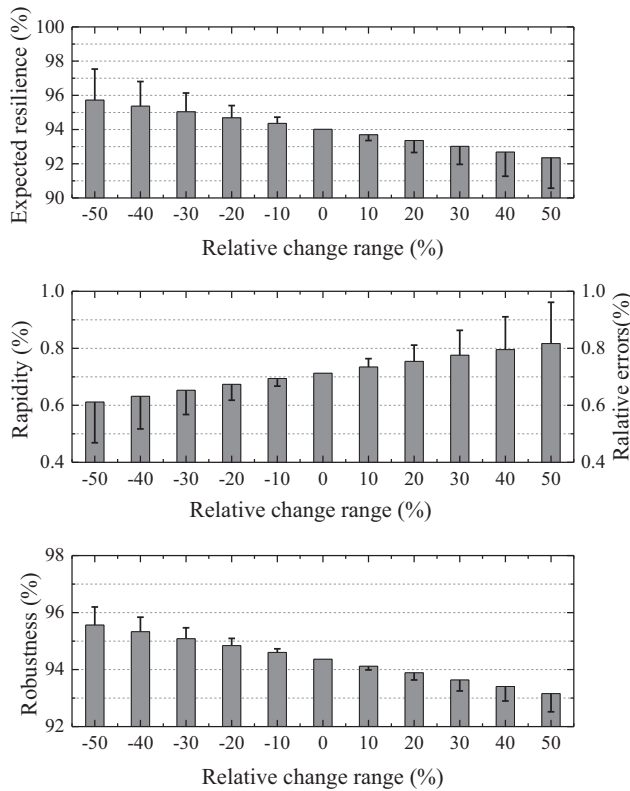


**Figure 12.** Moderate values and relative errors in 50 years of (a) expected resilience, (b) rapidity, and (c) robustness (RM)

bridge located in California, the following conclusions are drawn:

1. The occurrence proportions of NF and FF earthquakes have significant effects on the seismic hazard, seismic fragility, and functionality recovery function. Using the RM approach to integrate these three stages in the analysis procedure, the expected seismic resilience of bridges, including the impact of near-fault earthquakes, can be assessed.
2. The seismic resilience of the bridge in MR and SR conditions has been compared, and the relative error is about 4%, with more conservative results for MR.
3. Additional cases assuming the bridge is located in other near-fault regions are analyzed, changing the original occurrence proportion of NF and FF earthquakes to -50%—+ 50%. The maximum relative error for the expected resilience is nearly 2%, resulting in relative errors of about 10%.
4. The uncertainties of the parameters in the functionality recovery functions may affect the relative errors in using the SM conditions, reaching 15%. This indicates that the proposed method (RM) may significantly improve the accuracy of the seismic resilience assessment.

In conclusion, the proposed method is recommended for assessing the seismic resilience of bridges in near-fault regions. These results refer to a specific illustrative example

of a steel-concrete composite bridge and should be extended to other bridge typologies, even though they could represent a good starting point for investigation.

In fact, the calculation process and methodology presented in the paper can be used as a reference for exploring the effects on different types of bridges at the regional level, where an additional component vulnerability database is required. This certainly represents an interesting future extension of the present investigation.

## Acknowledgments

The authors would like to thank the editor and the anonymous reviewers for their constructive comments and valuable suggestions for improving the quality of the article. The financial support received from the National Science Foundation of China (Grant No. 52078176), the National Key Research and Development Program of China (Grant No. 2021YFB2600500), Wenzhou Basic Social Development Science and Technology Project (Grant No. S20220006), and Scientific Research Fund of Institute of Engineering Mechanics, China Earthquake Administration (Grant No. 2019D18) are gratefully appreciated. This study was also supported by FABRE – “Research Consortium for the Evaluation and Monitoring of Bridges, viaducts and other structures” ([www.conorziofabre.it/en](http://www.conorziofabre.it/en)).

This work was also carried out with a financial grant from the Research Fund for Coal and Steel of the European Community, within the SEQBRI project “Performance-Based Earthquake Engineering Analysis of Short-Medium Span Steel-Concrete Composite Bridges,” Grant RFSR-CT-2012-00032. Any opinion expressed in the paper does not necessarily reflect the view of the funder.

## References

- [1] Decò A, Bocchini P, Frangopol DM. A probabilistic approach for the prediction of seismic resilience of bridges. *Earth Eng Struct Dyn.* 2013;42(10):1469–1487.
- [2] Kalemli B, Caputo AC, Paolacci F, et al. A probabilistic framework for the estimation of resilience of process plants under Na-Tech seismic events. *Bull Earthq Eng.* 2024;22(1): 75–106. doi:10.1007/s10518-023-01685-z.
- [3] Bruneau M, Chang SE, Eguchi RT, et al. A framework to quantitatively assess and enhance the seismic resilience of communities. *Earthq Spectra.* 2003;19(4):733–752.
- [4] Bankoff G, Frerks G, Hilhorst D. *Mapping Vulnerability: Disasters, Development and People.* London: Earthscan; 2004.
- [5] Cimellaro GP, Reinhorn AM, Bruneau M. Seismic resilience of a hospital system. *Struct Infrastruct Eng.* 2010a;6(1–2):127–144.
- [6] Bruneau M, Reinhorn A. Exploring the concept of seismic resilience for acute care facilities. *Earthq Spectra.* 2007;23(1): 41–62.
- [7] Cimellaro GP, Reinhorn AM, Bruneau M. Framework for analytical quantification of disaster resilience. *Eng Struct.* 2010b;32(11):3639–3649.
- [8] Porter KA. An overview of PEER’s performance-based earthquake engineering methodology. In: *Proceedings of Ninth International Conference on Applications of Statistics and*

- Probability in Civil Engineering*; July 6–9, 2003; San Francisco, California, USA.
- [9] Federal Emergency Management Agency (FEMA). *Seismic Performance Assessment of Buildings Volume 1—Methodology, Technical Report FEMA-P58*. Washington, DC; 2012b.
  - [10] Echevarria A, Zaghi AE, Christenson R, et al. CFFT bridge columns for multihazard resilience. *J Struct Eng*. 2015;142(8):C4015002. doi:10.1061/(ASCE)ST.1943-541X.0001292.
  - [11] Karamlou A, Bocchini P. Computation of bridge seismic fragility by large-scale simulation for probabilistic resilience analysis. *Earthq Eng Struct Dyn*. 2015;44(12):1959–1978. doi:10.1002/eqe.2567.
  - [12] Xu N, Guikema SD, Davidson RA, et al. Optimizing scheduling of post-earthquake electric power restoration tasks. *Earthq Eng Struct Dyn*. 2007;36(2):265–284. doi:10.1002/eqe.623.
  - [13] Cimellaro GP, Malavisi M, Mahin S. Using discrete event simulation models to evaluate resilience of an emergency department. *J Earthq Eng*. 2016;21(2):203–226. doi:10.1080/13632469.2016.1172373.
  - [14] Bonstrom H, Corotis RB. First-order reliability approach to quantify and improve building portfolio resilience. *J Struct Eng*. 2014;142(8):C4014001. doi:10.1061/(ASCE)ST.1943-541X.0001213.
  - [15] Andrić JM, Lu D-G. Fuzzy methods for prediction of seismic resilience of bridges. *Int J Disaster Risk Reduct*. 2017;22:458–468, ISSN 2212–4209. doi:10.1016/j.ijdr.2017.01.001.
  - [16] Paredes R. A time-dependent seismic resilience analysis approach for networked lifelines; 2015.
  - [17] Dong Y, Frangopol DM, Saydam D. Time-variant sustainability assessment of seismically vulnerable bridges subjected to multiple hazards. *Earthq Eng Struct Dyn*. 2013;42(10):1451–1467.
  - [18] Reed DA, Kapur KC, Christie RD. Methodology for assessing the resilience of networked infrastructure. *IEEE Syst J*. 2009;3(2):174–180.
  - [19] Ouyang M, Dueñas-Osorio L. Time-dependent resilience assessment and improvement of urban infrastructure systems. *Chaos*. 2012;22(3):033122.
  - [20] Quinci G, Gagliardi V, Pallante L, et al. A novel bridge monitoring system implementing ground-based, structural and remote sensing information into a GIS-based catalogue. In: *Proceedings of SPIE—The International Society for Optical Engineering*, 2022; Berlin, 5–7 Sept 20. doi:10.1117/12.2637913.
  - [21] Alavi B, Krawinkler H. *Effects of Near-Fault Ground Motions on Frame Structures. Technical Report, Blume Center Report 138*. California: Stanford; 2001.
  - [22] Billah AM, Alam S, Bhuiyan MAR. Fragility analysis of retrofitted multi-column bridge bent subjected to near fault and far field ground motion. *J Bridge Eng*. 2013;18(10):992–1004.
  - [23] Baker JW. Quantitative classification of near-fault ground motions with wavelet analysis. *Bull Seismol Soc Am*. 2007;97(5):1486–1501.
  - [24] Bocchini P, Dan MF. Probabilistic Functionality Recovery Model for Resilience Analysis. In: *Bridge Maintenance, Safety, Management, Resilience and Sustainability*. 2012. p. 1920–1927. doi:10.1201/BMSM.
  - [25] Liu Y, Lu DG, Paolacci F. Probabilistic seismic resilience analysis for bridges shocked by near-fault pulse-like ground motions. In: *Maintenance, Monitoring, Safety, Risk and Resilience of Bridges and Bridge Networks*. CRC Press; 2016:230–231.
  - [26] Cornell CA, Jalayer F, Hamburger RO, et al. Probabilistic basis for 2000 SAC federal emergency management agency steel moment frame guidelines. *J Struct Eng*. 2002;128(4):526–533.
  - [27] Chang SE, Shinozuka M. Measuring improvements in the disaster resilience of communities. *Earthq Spectra*. 2004;20(3):739–755.
  - [28] Kafali C, Grigoriu M. 20Rehabilitation decision analysis. In: *ICOSSAR'05, Proceedings of the 9th International Conference on Structural Safety and Reliability, 19–23 June, 2005*; Rome, Italy.
  - [29] Mcguire RK. Probabilistic seismic hazard analysis and design earthquakes: closing the loop. *Int J Rock Mech Min Sci Geomech Abstr*. 1996;33(7):294A.
  - [30] Lin T, Baker JW. Probabilistic seismic hazard deaggregation of ground motion prediction models; 2011.
  - [31] Shahi SK. A probabilistic framework to include the effects of near-fault directivity in seismic hazard assessment (Doctoral dissertation, Stanford University); 2013.
  - [32] U.S. Geological Hazard Science Center. Accessed February 01, 2017. <https://geohazards.usgs.gov/deaggint/2008/>.
  - [33] Zhai C, Chang Z, Li S, et al. Quantitative identification of near-fault pulse-like ground motions based on energy. *Bull Seismol Soc Am*. 2013;103(5):2591–2603.
  - [34] Paolacci F, Corritore D. Performance-based earthquake engineering analysis of short-medium span steel-concrete composite bridges. In: *Italian Concrete Conference* (pp. 682–696); April 2021; Cham: Springer Nature Switzerland.
  - [35] Yang L, Paolacci F, Da-Gang L. Seismic fragility of a typical bridge using extrapolated experimental damage limit states. *Earthq Struct*. 2017;13(6):599–611. doi:10.12989/eas.2017.13.6.599.
  - [36] Chabrolin B, Kretz T, Laravoire J. *Steel-Concrete Bridges. A Guide for Novel Structures*. Paris: French National Project MIKTI; 2008.
  - [37] CEN. *Eurocode 8: Design of Structures for Earthquake Resistance, Part 1: General Rules, Seismic Actions and Rules for Buildings*. Brussels: European Committee for Standardization; 2005.
  - [38] McKenna F, Mazzoni S, Scott MH, et al. *OpenSees Command Language Manual*. Berkeley, July: Pacific Earthquake Engineering Research Center, University of California; 2007.
  - [39] Menegotto M, Pinto PE. Method of analysis for cyclically loaded RC plane frames including changes in geometry and non-elastic behavior of elements under combined normal force and bending. In: *Proceedings of IABSE Symposium on Resistance and Ultimate Deformability of Structures Acted on by Well Defined Repeated Loads*; 1973; Lisboa.
  - [40] Kent DC, Park R. Flexural members with confined concrete. *J Struct Div*. 1971;97(7):1969–1990.
  - [41] Liu Y, Paolacci F, Lu D. Seismic fragility of a typical bridge using extrapolated experimental damage limit states. *Earthq Struct*. 2017;13(6):599–611.
  - [42] CEN. *Eurocode 4: Design of Composite Steel and Concrete Structures*. Brussels: European Committee for Standardization; 2006.
  - [43] Gattesco N, Giuriani E. Experimental study on stud shear connectors subjected to cyclic loading. *J Constr Steel Res*. 1996;38(1):1–21.
  - [44] Abbiati G, Cazzador E, Alessandri S, et al. Experimental characterization and component-based modeling of deck-to-pier connections for composite bridges. *J Constr Steel Res*. 2018;50(1):31–50. doi:10.1016/j.jcsr.2018.08.005.

- [45] Bradley B. The seismic demand hazard and importance of the conditioning intensity measure. *Earthq Eng Struct Dyn.* 2012;41:1417. doi:10.1002/eqe.2221.
- [46] De Biasio M, Grange S, Dufour F, et al. Intensity measures for probabilistic assessment of non-structural components acceleration demand. *Earthq Eng Struct Dyn.* 2015;44(13):2261–2280. doi:10.1002/eqe.2582.
- [47] Shome N, Cornell CA, Bazzurro P, et al. Earthquakes, records, and nonlinear responses. *Earthq Spectra.* 1998;14(3):469–500.
- [48] Giovenale P, Cornell C, Esteva L. Comparing the adequacy of alternative ground motion intensity measures for the estimation of structural responses. *Earthq Eng Struct Dyn.* 2004;33(8):951–979.
- [49] U.S. geological hazard science center. 2017b. Accessed 15 January 2017. <https://earthquake.usgs.gov/hazards/qfaults/map/#qfaults>.
- [50] Yong A, Thompson EM, Wald D, et al. Compilation of Vs30 data for the United States: U.S. Geological Survey Data Series 978, 8 p.
- [51] Shahi SK, Baker JW. An empirically calibrated framework for including the effects of near-fault directivity in probabilistic seismic hazard analysis. *Bull Seismol Soc Am.* 2011;101(2):742–755.
- [52] Chioccarelli E, Iervolino I. Near-source seismic hazard and design scenarios. *Earthq Eng Struct Dyn.* 2013;42(4):603–622.
- [53] U.S. Geological Hazard Science Center. 2017c. Accessed February 01, 2017. <http://geohazards.usgs.gov/hazardtool/application.php>.
- [54] Ancheta TD, Darragh RB, Stewart JP et al. *PEER NGA-West2 Database, PEER Report 2013/03*. Berkeley: Pacific Earthquake Engineering Research Center. University of California; 2013.
- [55] Stewart JP, Chiou SJ, Bray JD, et al. Ground motion evaluation procedures for performance-based design. *Soil Dyn Earthq Eng.* 2002;22(9):765–772.
- [56] Bray JD, Rodriguez-Marek A. Characterization of forward-directivity ground motions in the near-fault region. *Soil Dyn Earthq Eng.* 2004;24(11):815–828.
- [57] Padgett JE. Selection of optimal intensity measures in probabilistic seismic demand models of highway bridge portfolios. *Earthq Eng Struct Dyn.* 2008;37(5):711–725.
- [58] Wen YK, Ellingwood BR, Veneziano D, et al. Uncertainty modeling in earthquake engineering. MAE center project FD-2 report; 2003.
- [59] Baker JW, Lin T, Shahi SK, Jayaram N. New ground motion selection procedures and selected motions for the PEER transportation research program. *Peer Rep.* 2011; 2011:3.
- [60] Tothong P, Cornell CA. Structural performance assessment under near-source pulse-like ground motions using advanced ground motion intensity measures. *Earthq Eng Struct Dyn.* 2008;37(37):1013–1037.
- [61] Paolacci F, Corritore D. Performance-based earthquake engineering analysis of short-medium span steel-concrete composite bridges. In: *Lecture Notes in Civil Engineering, Volume 351, Pages 682–696, 2023 Italian Concrete Conference, ICC 2021, Virtual, Online 14 April 2021 through 17 April 2021*; 2023. doi:10.1007/978-3-031-37955-0\_49.
- [62] Muntasir Billah AHM, Shahria Alam M. Seismic fragility assessment of highway bridges: a state-of-the-art review. *Struct Infrastruct Eng.* 2015;11(6):804–832.
- [63] Stefanidou SP, Kappos AJ. Methodology for the development of bridge-specific fragility curves. *Earthq Eng Struct Dyn.* 2017;46(1):73–93.
- [64] Tirca L, Serban O, Lin L, et al. Improving the seismic resilience of existing braced-frame office buildings. *J Struct Eng.* 2015;142(8):C4015003.
- [65] Shinozuka M, Zhou Y, Kim SH, et al. Socio-economic effect of seismic retrofit implemented on bridges in the Los Angeles highway network. Final Report to the California Department of Transportation; 2005.
- [66] HAZUS. *MR4 Earthquake Model Technical Manual*. Washington (DC): Department of Homeland Security, Federal Emergency Management Agency, Mitigation Division; 2009.
- [67] ATC. *Earthquake Damage Evaluation Data for California. Technical Report ATC-13*. Redwood City, CA: Applied Technology Council (ATC); 1985.